ACS OMEGA

Open Access

http://pubs.acs.org/journal/acsodf

Article

Theoretical Exploration of Enhanced Antioxidant Activity in Copper Complexes of Tetrahydroxystilbenes: Insights into Mechanisms and Molecular Interactions

Salima Hamadouche, Hafida Merouani, Abd Alghani May, Nadia Ouddai, Manawwer Alam, Luca Micoli, Alessandro Erto, and Yacine Benguerba*

Cite This: *ACS Omega* 2024, 9, 9076−9089

Read Online

ACCESS | Metrics & More | Article Recommendations

ABSTRACT: A theoretical investigation was conducted using DFT/PW91/TZP/DMSO calculations on a complete set of exhaustive lists of 18 compounds resulting from the complexation of *trans*-2,4,3′,5′-tetrahydroxystilbene (T-OXY) and *cis*-2,4,1′,3′-tetrahydroxystilbene (C-OXY) with copper metal cations (Cu^+ and Cu^{2+}). The ligand-binding sites are the critical points of Quantum Theory of Atoms in Molecules (QTAIM) analysis on neutral and deprotonated ligands. Various mechanisms, including hydrogen atom transfer (HAT), sequential proton loss electron transfer (SPLET), single electron transfer followed by proton transfer (SET-PT), and bond dissociation energy (BDE(E0)) calculations, were employed to quantify the antioxidant activity. The BDE(E0) mechanism emerged as the most suitable approach for such analyses to evaluate the departure of hydrogen atoms since the results show the HAT mechanism is the most likely occurring. Particularly intriguing were the anionic Cu^+ complexes with ligands adopting trans configurations and deprotonated conformations, displaying superior antioxidant activity compared to their counterparts. Remarkably, a single ligand within the Cu^+ complex exhibited exceptional antioxidant prowess, yielding a BDE(E0) value of 91.47 kcal/mol. Furthermore, a complex involving two deprotonated ligands demonstrated antioxidant activity of 31.12 kcal/mol, signifying its potential as a potent antiradical agent, surpassing T-OXY by a factor of 3.91 and even surpassing the antioxidant efficiency of Vitamin C.

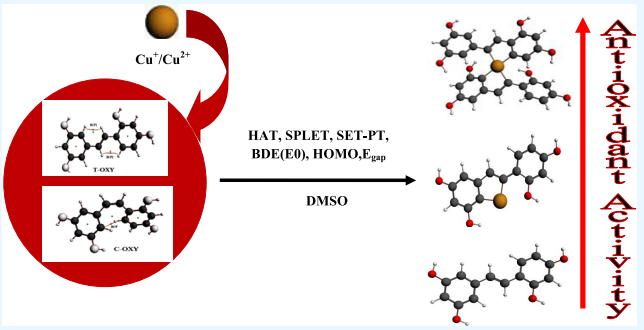

1. INTRODUCTION

2,4,3′,5′-Tetrahydroxystilbene (Oxyresveratrol; OXY)[1] is a naturally occurring hydroxystilbene found in plants, notably in mulberry wood.[2] It exists in two isomers: trans (T-OXY) and cis (C-OXY).[3] OXY demonstrates a spectrum of compelling biological activities, including antiherpetic and anti-HIV effects,[2] anti-inflammatory,[4] antiapoptotic and neuroprotective,[5] and, particularly, potent antioxidant capabilities.[1,6] Our prior theoretical investigation revealed that T-OXY outperforms its cis-isomer in scavenging long- and short-lived free radicals.[1] Its scavenging potential follows the sequence: $HO^\bullet \gg CH_3O^\bullet > HOO^\bullet > CH_3OO^\bullet > NO_2^\bullet > NO^\bullet$[1,7] Additionally, the Quantum Theory of Atoms in Molecules (QTAIM) descriptors and the corresponding Bond Critical Points (BCPs) were reported, with two BCPs identified for T-OXY and one for C-OXY (see Figure 1).[7]

The critical point in (C-OXY) leads to a complexation, or Diels−Alder cyclization type, resulting in two products, T-CYCLE-OXY and C-CYCLE-OXY, with antiradical activities of 97.79 and 101.08 kcal/mol, respectively.[7] For the trans geometry, the two critical points indicate a probability of complexation between T-OXY and a transition metal. These metal complexes can potentially exhibit enhanced antioxidant capabilities, such as flavonoid complexes that have demonstrated superior efficiency in radical inhibition.[8−10] To further enhance the antioxidant prowess of OXY, we propose its complexation with transition metals. A diverse array of geometries, coordination numbers, and oxidation states can be achieved.[11,12] The selection of the metal and the choice of mechanism play a significant role in boosting antioxidant capacity.[13,14] Experimental and theoretical studies have identified two well-distinct complexation mechanisms: direct chelation and coupled-deprotonation-chelation, with the latter being considered more plausible.[15,16] Copper complexes have

Received: October 9, 2023
Revised: January 25, 2024
Accepted: January 29, 2024
Published: February 12, 2024

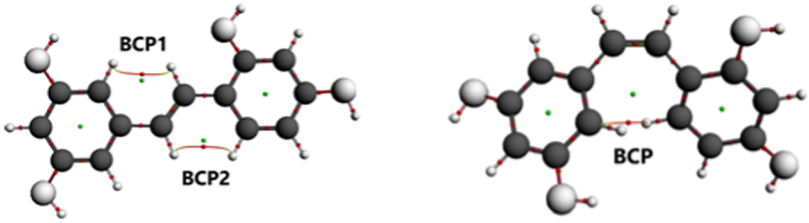

Figure 1. Graphic representation of bond critical points (BCPs in red) and ring critical points (RCPs in green) of T-OXY and C-OXY with QTAIM analysis by PW91/TZP in DMSO.

attracted significant interest due to their remarkable anticancer and antioxidant properties, surpassing those of nickel, cobalt, and zinc complexes.[17−25] Encouraging outcomes from joint experimental and theoretical studies on copper-resveratrol complexes[26,27] have motivated us to explore the complexation of OXY with copper in its two oxidation states, Cu^{+} and Cu^{2+}. To the best of our knowledge, complexes of Cu^{+} and Cu^{2+} with the ligand Resveratrol substituted by OH in position (5′) have not been determined experimentally.

2. COMPUTATIONAL DETAILS

In this work, we applied the QTAIM results for the complexation of Cu^{+} and Cu^{2+} with T-OXY and C-OXY by two mechanisms. Table 1 shows the terminology that was used.

In the first, the ligands exist in their neutral state, and their binding with Cu^{+} and Cu^{2+} metal ions leads to the formation of positively charged complexes. The second mechanism involves the deprotonation of ligands at their respective critical points, yielding negatively charged ligands (−2). Lastly, for the first time, the coordination of two neutral and deprotonated OXY ligands charged (−4) with Cu^{+} and Cu^{2+}. The influence of complexation on OXY's antioxidant capabilities of OXY through these two pathways was evaluated quantitatively, and the most effective antioxidant site and complex within the DMSO solvent were determined through this process. These mechanisms include the bond dissociation energy BDE(E0) approach; this method is based on the cleavage of the O−H bond intramolecularly by homolytic fragmentation, as well as by (I) hydrogen atom transfer (HAT), which takes place in a single step from the antioxidant molecule to the radical;[28] (II) single electron transfer followed by proton transfer (SET-PT), which takes place in two steps: the initial formation of a cationic radical by transferring an electron from the antioxidant to the free radical and then a proton transfer from the cation radical to the anion; and (III) sequential proton loss electron transfer (SPLET) comprises two consecutive steps: deprotonation of the antioxidant (anion formation) followed by electron transfer to the free radical. Key thermochemical metrics such as bond dissociation enthalpies (BDE), adiabatic ionization potentials (IP), proton dissociation enthalpies (PDE), proton affinities (PA), and electron transfer enthalpy (ETE) energies are used to assess these processes (enthalpies of electron transfer). (SET-PT) and (SPLET) are based on the potential of the antioxidant molecule to donate an electron and are hard to distinguish.[29] This trifecta of processes competes with one another.[7,30] Another crucial electrical characteristic for determining a molecule's propensity to participate in electron transfer processes is its highest occupied molecular orbital (HOMO) energy level. Our previous research[7] established T-OXY as the best antioxidant available. Therefore, we also compare it here.

Table 1. Nomenclature Used for the Cu^{+} and Cu^{2+} Complexes

	type	code name
Cu^{+} Complexes		
Cu^{+} with neutral T-OXY on the BCP P1 critical point via oxygen	positively charged	$[Cu_{P1}{}^{+}-(T\text{-}OXY)]^{+}$
Cu^{+} with neutral T-OXY on the critical point BCP P1 via carbon		$[Cu_{P1}{}^{+}-(T\text{-}OXY)]^{+\prime}$
Cu^{+} with neutral T-OXY on the critical point BCP P2		$[Cu_{P2}{}^{+}-(T\text{-}OXY)]^{+}$
Cu^{+} with neutral C-OXY at the BCP critical point		$[Cu^{+}-(C\text{-}OXY)]^{+}$
Cu^{+} with T-OXY deprotonated at the BCP P1 critical point	negatively charged	$[Cu_{P1}{}^{+}-(T\text{-}OXY)_{dep}^{-2}]^{-}$
Cu^{+} with T-OXY deprotonated at the BCP P2 critical point		$[Cu_{P2}{}^{+}-(T\text{-}OXY)_{dep}^{-2}]^{-}$
Cu^{+} with C-OXY deprotonated at the BCP critical point		$[Cu^{+}-(C\text{-}OXY)_{dep}^{-2}]^{-}$
Cu^{+} with two neutral T-OXY at their critical points	two neutral and deprotonated OXY	$[Cu^{+}-2(T\text{-}OXY)]^{+}$
Cu^{+} with two T-OXY deprotonated at their critical points		$[Cu^{+}-2(T\text{-}OXY)_{dep}^{2-}]^{-3}$
Cu^{2+} Complexes		
Cu^{2+} with neutral T-OXY at the BCP P1 critical point via oxygen	positively charged	$[Cu_{P1}{}^{2+}-(T\text{-}OXY)]^{2+}$
Cu^{2+} with neutral T-OXY on the critical point BCP P1 via carbon		$[Cu_{P1}{}^{2+}-(T\text{-}OXY)]^{2+\prime}$
Cu^{2+} with neutral T-OXY at the critical point BCP P2		$[Cu_{P2}{}^{2+}-(T\text{-}OXY)]^{2+}$
Cu^{2+} with neutral C-OXY at the BCP critical point		$[Cu^{2+}-(C\text{-}OXY)]^{2+}$
Cu^{2+} with T-OXY deprotonated at the BCP P1 critical point	negatively charged	$[Cu_{P1}{}^{2+}-(T\text{-}OXY)_{dep}^{-2}]$
Cu^{2+} with T-OXY deprotonated at the BCP P2 critical point		$[Cu_{P2}{}^{2+}-(T\text{-}OXY)_{dep}^{-2}]$
Cu^{2+} with deprotonated C-OXY on the BCP critical point		$[Cu^{2+}-(C\text{-}OXY)_{dep}^{-2}]$
Cu^{2+} with two neutral T-OXYs at their critical points	two neutral and deprotonated OXY	$[Cu^{2+}-2(T\text{-}OXY)]^{2+}$
Cu^{2+} with two deprotonated T-OXY (charged −4) on their critical points		$[Cu^{2+}-2(T\text{-}OXY)_{dep}^{2-}]^{-2}$

The structures of copper complex compounds were optimized by density functional theory (DFT) calculations,[31] using Amsterdam Density Functional (ADF) software,[32] as well as single-point calculations. The PW91 level (Perdew−Wang 1991),[33] the functional GGA (Generalized Gradient Approximation) exchange−correlation function, and the Slater TZP (Triple zeta polarization) set of atomic bases,[34] valence orbitals of all atoms (1s for H; 2p for O and C; and 4s, 3d for Cu). Medium frozen cores were retained for the internal

https://doi.org/10.1021/acsomega.3c07885
ACS Omega 2024, 9, 9076−9089

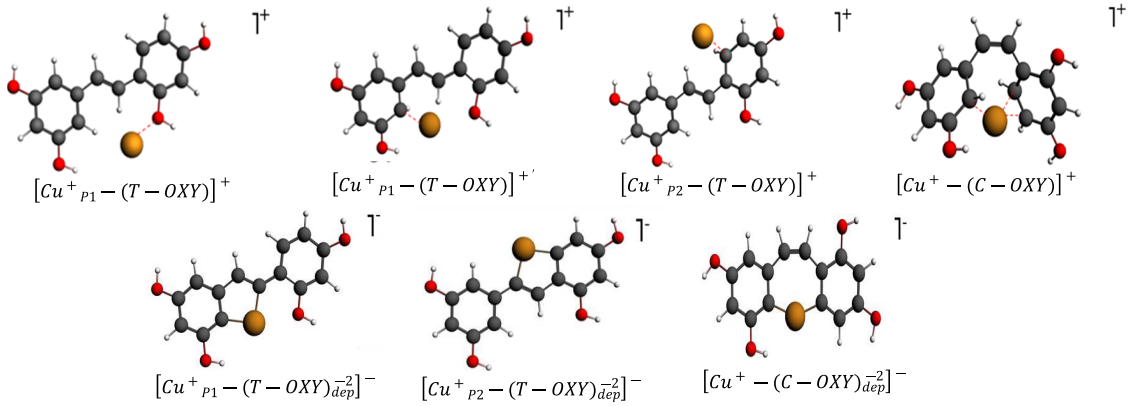

Figure 2. Optimized structures using computational level DFT/PW91/TZP/DMSO of Cu^{+} complexes with mono-2,4,3′,5′-tetrahydroxystilbene neutral and deprotonated at the binding sites.

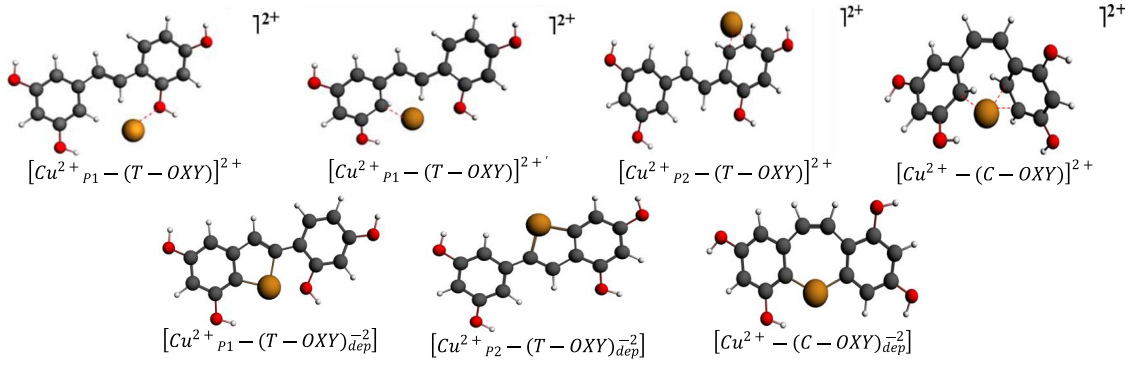

Figure 3. Optimized structures using computational level DFT/PW91/TZP/DMSO of Cu^{2+} complexes with mono-2,4,3′,5′-tetrahydroxystilbene neutral and deprotonated at the binding sites.

orbitals. The Becke parameter is used for integration, and the energy convergence threshold is set at 1×10^{-3} atomic units. The COSMO solvent effect was utilized to simulate the impact of DMSO, as implemented in ADF,[35] characterized by a dielectric constant (ε) of 46.7 and van der Waals radii of 3.04 Å. Since the copper-OXY complexes lack an X-ray structure, their structures were generated using the graphical interface of the program. To enhance the accuracy of the computations, it was ensured that all optimized structures had reached the potential energy surface's global minimum, indicated by a zero imaginary frequency.

3. ANTIOXIDANT ACTIVITY DESCRIPTOR

3.1. Bond Dissociation Energy (BDE(E0)) Analysis. The energy required for the intramolecular homolytic cleavage of the O−H chemical bonds indicates a molecule's antioxidant effectiveness. The procedure specified in the ADF code took a few steps: we perform the fragment calculation based on the regions panel that $ArO^{\bullet}$ defines as one and the H atoms as the other in all of the locations. The next step is to run a single-point calculation with ADF and view the results. Finally, intermolecular interactions are separated in terms of specific energy, and the expression calculates the bond dissociation energy:

$$\mathrm{BDE}(E0) = E_{\mathrm{elect}} + E_{\mathrm{Pauli}} + E_{\mathrm{orb}} = E_{\mathrm{elect}} + E_{(\mathrm{Pauli+orb})} \quad (1)$$

where E_{elect} is the electrostatic energy used to qualify the electrostatic interaction between the two fragments; E_{Pauli} is the Pauli energy, a destabilizing component linked to the repulsive interactions between fragments; and E_{orb} is the orbital interaction that can be summarized in the framework of the single electronic approximation as the sum of the stabilizing interactions with 2 electrons and two orbitals. The contributions of E_{Pauli} sand E_{orb} are generally grouped in $E_{(\mathrm{Pauli+orb})}$.[36]

3.2. Antioxidant Property Descriptors. Enthalpies (H) at 298.15 K were used to obtain the following quantities: BDE, IP, PDE, PA, and ETE:

$$\mathrm{BDE} = H(\mathrm{ArO}^{\bullet}) + H(\mathrm{H}^{\bullet}) - H(\mathrm{ArOH}) \quad (2)$$

$$\mathrm{IP} = H(\mathrm{ArOH}^{\bullet+}) + H(\mathrm{e}^{-}) - H(\mathrm{ArOH}) \quad (3)$$

$$\mathrm{PDE} = H(\mathrm{ArO}^{\bullet}) + H(\mathrm{H}^{+}) - H(\mathrm{ArOH}^{\bullet+}) \quad (4)$$

$$\mathrm{PA} = H(\mathrm{ArO}^{-}) + H(\mathrm{H}^{+}) - H(\mathrm{ArOH}) \quad (5)$$

$$\mathrm{ETE} = H(\mathrm{ArO}^{\bullet}) + H(\mathrm{e}^{-}) - H(\mathrm{ArO}^{-}) \quad (6)$$

Low BDE levels indicate the antioxidant's ability to generate hydrogen through interaction with radicals, demonstrating a high level of antioxidant activity and the presence of the HAT mechanism.[37] The IP and PDE levels play a role in determining the success of SET-PT. If the IP values (first-step reaction) are high, then the SET-PT method is not preferred. PDE refers to the second step in the SET-PT mechanism. Lower values of PA and ETE favor the SPLET mechanism (PA: the enthalpy of the reaction in the first step; ETE: the enthalpy of the reaction in the second step).

https://doi.org/10.1021/acsomega.3c07885
ACS Omega 2024, 9, 9076−9089

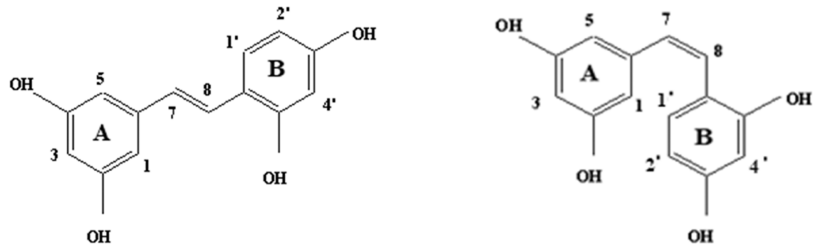

Figure 4. Chemical structures of *cis*- and *trans*-OXY.

Antioxidant molecules are found in physiological fluids in vivo (polar media). The calculated enthalpies of electrons (e^-), protons (H^+), and hydrogen atoms ($H^\bullet$) in DMSO are 1.19, −20.07, and −266.49 kcal/mol, respectively.[38]

4. RESULTS AND DISCUSSION

C-OXY and T-OXY consist of two aromatic rings connected by an ethylene bridge, positioning them among the top-performing antioxidants.[39,40] Our investigation focused on the coordination of Cu^+ and Cu^{2+} ions with T-OXY and C-OXY, involving an analysis of multiple parameters.

4.1. Structural parameters. For this theoretical study, our choice of calculations at the PW9/TZP theoretical level is not arbitrary. The calculated bond lengths and angles strongly correlated with those observed experimentally for the organometallic complexes in our previous theoretical studies, indicating the accuracy and reliability of the computational methods used.[41−43] No available crystallographic structural data detailing complexes formed between *cis*- and *trans*-OXY and Cu^+ or Cu^{2+} ions exist. Illustratively, Figures 2 and 3 visually convey the diverse configurations that emerged from the coordination of metal ions at the sites of critical points by the two proposed mechanisms, respectively.

The initial four structures were derived using a direct chelation approach, where no restrictions were placed on the ligands. In this method, either Cu^+ or Cu^{2+} is positioned at the critical point, creating a bond with the neutral OXY ligand. In contrast, the last three systems, presented in both figures, were obtained by applying a specific constraint: the coupled-deprotonation coordination of Cu^+ or Cu^{2+} at the critical point. These visual representations provide a clear understanding of the complex coordination interactions, offering insights into the diverse configurations that emerge from different binding scenarios.

4.1.1. Molecular Geometries. Many studies correlate polyphenols' antioxidant capacity and molecular structure.[44−46] Their significant antioxidant capabilities distinguish *cis*- and *trans*-OXY, attributed to their structure consisting of two aromatic rings linked by an ethylene unit. This arrangement positions them among the most effective antioxidants[47] (Figure 4).

Our investigation involves an analysis of the coordination of Cu^+ and Cu^{2+} ions to T-OXY and C-OXY. This analysis encompasses several structural parameters of the configuration optimized at the PW91/TZP/DMSO level of theory of: $[Cu_{P1}{}^+-(T\text{-}OXY)]^+$, $[Cu_{P1}{}^+-(T\text{-}OXY)]^{+\prime}$, $[Cu_{P2}{}^+-(T\text{-}OXY)]^+$, $[Cu^+-(C\text{-}OXY)]^+$, $[Cu_{P1}{}^+-(T\text{-}OXY)_{dep}^{-2}]^-$, $[Cu_{P2}{}^+-(T\text{-}OXY)_{dep}^{-2}]^-$, $[Cu^+-(C\text{-}OXY)_{dep}^{-2}]^-$, $[Cu_{P1}{}^{2+}-(T\text{-}OXY)]^{2+}$, $[Cu_{P1}{}^{2+}-(T\text{-}OXY)]^{2+\prime}$, $[Cu_{P2}{}^{2+}-(T\text{-}OXY)]^{2+}$, $[Cu^{2+}-(C\text{-}OXY)]^{2+}$, $[Cu_{P1}{}^{2+}-(T\text{-}OXY)_{dep}^{-2}]$, $[Cu_{P2}{}^{2+}-(T\text{-}OXY)_{dep}^{-2}]$, $[Cu^{2+}-(C\text{-}OXY)_{dep}^{-2}]$. All data regarding these parameters can be found in Table 2, which summarizes the pertinent values for bond lengths, angles, and optimized dihedral angles in the Cu^{2+} and Cu^+ complexes. Across all complex structures, the characteristic double bond nature of the ethylenic bridge, as seen in stilbenes, is retained and designated as $C_7{=}C_8$ in column 1 − bond lengths such as C_7-C_6 and $C_8-C_{6'}$ range from 1.391 to 1.455 Å. Notably, the average bond lengths within the aromatic rings A and B (indicated in columns C_A-C_A and C_B-C_B) within the complex geometries are approximately 1.4 Å, highlighting π electron delocalization and electronic resonance in these aromatic rings.[48] This resonance phenomenon mirrors the behavior seen in the T-OXY and C-OXY compounds. Additionally, bond lengths such as $O_{5'}-H_{5'}$, $O_{3'}-H_{3'}$, O_2-H_2, and O_4-H_4 within the aromatic rings remain relatively constant, fluctuating between 0.980 and 0.991 Å. The planar structure is a pivotal determinant of superior antioxidant activity,[26] enabling facile hydrogen detachment and electron transfer.[27] This attribute contributes to the stability of the radical, anionic, and cationic forms after oxidation. However, this planar feature is absent for one or both sides in the geometries of $[Cu^+-(C\text{-}OXY)]^+$, $[Cu^{2+}-(C\text{-}OXY)]^{2+}$, $[Cu_{P2}{}^+-(T\text{-}OXY)]^+$, $[Cu_{P2}{}^{2+}-(T\text{-}OXY)]^{2+}$, $[Cu_{P1}{}^+-(T\text{-}OXY)]^{+\prime}$, and $[Cu_{P1}{}^{2+}-(T\text{-}OXY)]^{2+\prime}$, where coordination occurs through the ring carbon. The C−Cu bond length varies from 1.873 to 1.976 Å, and $C_{ph}-Cu$ ranges from 1.877 to 1.962 Å, discrepancies of (0.01−0.04) are noted compared to experimental bond length values. Cu^+ and Cu^{2+} chelate via oxygen in both $[Cu_{P1}{}^+-(T\text{-}OXY)]^+$ and $[Cu_{P1}{}^{2+}-(T\text{-}OXY)]^{2+}$ complexes, forming a dative bond involving oxygen's electron pair and copper's vacant orbital. The length of this bond ranges from 1.984 to 2.044 Å.[27] The location of the (QTAIM) Bond Critical Points (BCPs) was the motive for placing cations at these locations. The results indicate that copper cations coordinate via phenolic carbons or C=C double bonds, except in two structures, where cations are bound to an OH group. Similarly, experimental and theoretical findings in studies[26,27] reveal the coordination method of copper with Resveratrol, a member of the same family as OXY, in these positions.

Figure 5 depicts the molecular structures of Cu^{2+} and Cu^+ complexes with a single neutral *trans* and *cis* ligand.

In the molecular structure of complexes with single neutral cis and trans ligands, coordination with copper ions occurs through oxygen atoms and ring carbon at critical point 1 and exclusively through ring carbon atoms at critical point 2, with coordination modes $\eta = 1$ for Cu^+ and $\eta = 2$ for Cu^{2+} in the latter. This pattern is also observed in the cis geometry, where the coordination modes are $\eta = 3$ for both Cu^+ and Cu^{2+}. In the case of charged, bis-deprotonated ligands (2-), the coordination to copper atoms is via carbon atoms, with $\eta = 3$ for Cu^{2+} and $\eta = 4$ for Cu^+. The four copper complexes feature Cu^{2+} and Cu^+ coordinated with two ligands in their deprotonated and saturated forms, respectively, as illustrated in

https://doi.org/10.1021/acsomega.3c07885
ACS Omega 2024, 9, 9076−9089

Table 2. Bond Lengths (Å), Bond angles (deg), and Dihedral Angles (deg) for the Target Complexes Optimized at the PW91/TZP Level of Theory in DMSO[a]

compounds	$C_7{=}C_8$	$C_7{-}C_6$	$C_8{-}C_{6'}$	$C_A{-}C_A$	$C_B{-}C_B$	$O_{5'}{-}H_{5'}$	$O_{3'}{-}H_{3'}$	$O_2{-}H_2$	$O_4{-}H_4$	O−Cu	$Cp_h{-}Cu$	C−Cu	C−Cu−C	α ($C_8C_1{'}C_{6'}C_7$)	$\theta(C_7C_1C_6C_8)$	ref
T-OXY	1.346	1.446	1.440	1.390	1.391	0.980	0.980	0.980	0.980					2.1	3	7
C-OXY	1.350	1.453	1.447	1.390	1.392	0.981	0.982	0.980	0.980					8	12	7
							Cu^+ Complexes									
$[Cu_{P1}{}^+{-}(T\text{-}OXY)]^+$	1.353	1.437	1.413	1.391	1.392	0.984	0.982	0.982	0.981	2.044				2	2.6	
$[Cu_{P1}{}^+{-}(T\text{-}OXY)]^{+\prime}$	1.377	1.416	1.412	1.408	1.394	0.982	0.982	0.986	0.986		1.979			0	14.9	
$[Cu_{P2}{}^+{-}(T\text{-}OXY)]^+$	1.361	1.429	1.414	1.392	1.402	0.981	0.981	0.981	0.980		1.994			9	10.5	
$[Cu^+{-}(C\text{-}OXY)]^+$	1.375	1.436	1.423	1.405	1.406	0.983	0.982	0.983	0.981		1.989	1.975	109.0	14	14	
$[Cu_{P1}{}^+{-}(T\text{-}OXY)_{dep}^{-2}]^-$	1.369	1.450	1.422	1.398	1.396	0.982	0.980	0.991	0.980		1.943	1.947	93.2	1.7	0	
$[Cu_{P2}{}^+{-}(T\text{-}OXY)_{dep}^{-2}]^-$	1.373	1.431	1.448	1.395	1.398	0.980	0.982	0.980	0.980		1.948	1.944	97.0	0.1	0.7	
$[Cu^+{-}(C\text{-}OXY)_{dep}^{-2}]^-$	1.397	1.437	1.437	1.399	1.401	0.980	0.980	0.988	0.979		1.877	1.876	141.8	0.5	0.3	
							Cu^{2+} Complexes									
$[Cu_{P1}{}^{2+}{-}(T\text{-}OXY)]^{2+}$	1.363	1.426	1.391	1.394	1.396	0.985	0.983	0.982	0.981	1.984				1	3.9	
$[Cu_{P1}{}^{2+}{-}(T\text{-}OXY)]^{2+\prime}$	1.373	1.424	1.404	1.403	1.397	0.983	0.985	0.984	0.985		1.993			1	17.1	
$[Cu_{P2}{}^{2+}{-}(T\text{-}OXY)]^{2+}$	1.371	1.416	1.408	1.394	1.407	0.983	0.983	0.981	0.982		2.040	2.001	40.7	10.4	6.8	
$[Cu^{2+}{-}(C\text{-}OXY)]^{2+}$	1.365	1.441	1.417	1.404	1.409	0.985	0.984	0.983	0.983		1.982	1.969	109.3	14	16	
$[Cu_{P1}{}^{2+}{-}(T\text{-}OXY)_{dep}^{-2}]$	1.339	1.455	1.423	1.394	1.391	0.983	0.985	0.987	0.981		1.929	1.976	87.5	0.5	0.2	
$[Cu_{P2}{}^{2+}{-}(T\text{-}OXY)_{dep}^{-2}]$	1.348	1.441	1.445	1.391	1.392	0.981	0.983	0.980	0.980		1.939	1.956	91.8	0.3	3.4	
$[Cu^{2+}{-}(C\text{-}OXY)_{dep}^{-2}]$	1.360	1.455	1.445	1.393	1.394	0.982	0.983	0.985	0.980		1.877	1.873	123.5	1.7	5	

[a] $C_A{-}C_A$ is the average of the bond lengths of the phenolic ring A of the structure; CB−CB is the average of the bonding lengths of phenolic ring B of the structure; $*p_h{-}Cu$: bond length between ring carbon and copper.

https://doi.org/10.1021/acsomega.3c07885
ACS Omega 2024, 9, 9076−9089

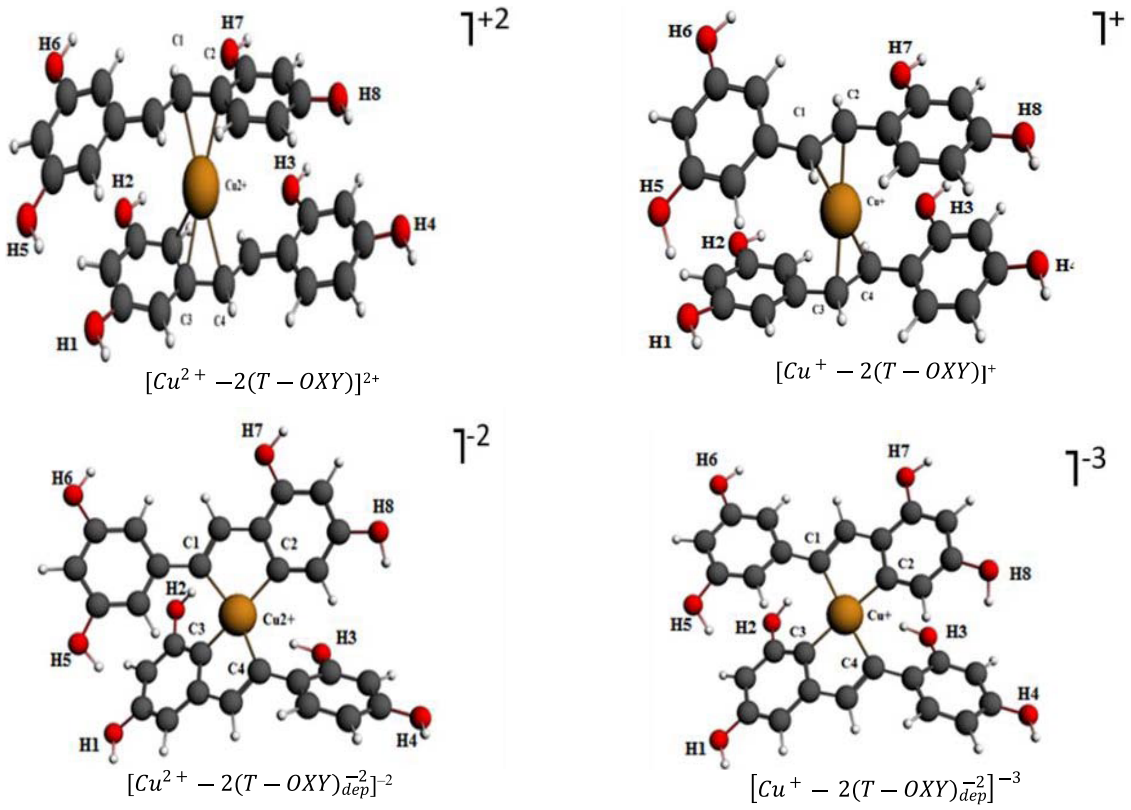

Figure 5. Optimized structures of Cu^{+} and Cu^{2+} complexes with bi-2,4,3′,5′-tetrahydroxystilbene neutral and deprotonated by PW91/TZP in DMSO.

Figure 5. Selected bond distances, angles, and dihedral angles are listed in Table 3. The DFT study indicates that deprotonated OXY acts as a bidentate ligand, coordinating through the ethylenic bridge's carbons and the cycle. For neutral ligands, the bond lengths are for [Cu^{2+}−C = 2.079−2.167 Å and Cu^{+}−C = 2.045−2.068 Å] and coordinate to Copper Cu^{2+} and Cu^{+} by (η = 5 and η = 4), respectively. However, for the deprotonated ligands, the bond lengths are for [Cu^{2+}−C = 1.966−2.060 Å and Cu^{+}−C = 1.953−2.066 Å] and coordinate to copper Cu^{2+} and Cu^{+} by (η = 4), respectively. The two complexes [Cu^{2+}−2(T-OXY)]$^{2+}$ and [Cu^{+}−2(T-OXY)]$^{+}$, adopt a square-based pyramid geometry. While the complexes [Cu^{2+}−2(T-OXY)$^{-2}_{dep}$]$^{-2}$ and [Cu^{+}−2(T-OXY)$^{-2}_{dep}$]$^{-3}$ adopt a pseudo-square planar geometry. It is also apparent from the O−H distance of the eight sites is more or less constant and varies from 0.976 to 1.022 Å.

4.2. Mechanistic Study of Antioxidant Property. The choice of the mechanism among HAT, SET-PT, or SPLET, given the number and size of 18 complexes in our list, with all of their O−H sites, will cost us time and computational materials. We thought of choosing from this list two example compounds: [$Cu_{P1}{}^{+}$−(T-OXY)$^{-2}_{dep}$]$^{-}$, as complex with a single ligand, and [Cu^{+}−2(T-OXY)$^{-2}_{dep}$]$^{-3}$, as compounds with two ligands. Our previous study's BDE($E0$) and other antioxidant descriptor outcomes indicated that OXY's most potent antioxidant activity sites of OXY are on the B ring. This rationalizes our focus on the 5′-OH and 4-OH sites. Table 4 provides a comprehensive summary of the computed properties of all compounds, including their radical, anionic, and cationic forms in the DMSO solvent. The distinct energies in determining the preferable mechanism of antioxidant action provide a highly objective analysis. The BDE is a reliable thermochemical measure for characterizing the HAT process, wherein an H atom transfers from the hydroxyl group of the antioxidant molecule to a free radical. The weakest O−H bond, indicated by the lowest BDE value, is expected to drive the most probable reaction and exhibit the highest antioxidant activity. Our results highlight that [$Cu_{P1}{}^{+}$−(T-OXY)$^{-2}_{dep}$]$^{-}$ and [Cu^{+}−2(T-OXY)$^{-2}_{dep}$]$^{-3}$ exhibit the lowest BDE values at the 5′-OH and 4-OH sites, measuring 64.13 and 29.23 kcal/mol, respectively. The ease of H atom removal from these positions suggests the most stable radical formation. Hence, both complexes preferentially engage in the HAT mechanism, with the ethylenic bridge contributing to radical stabilization in the antioxidant form.[45,49]

The cationic radical $ArOH^{+}$ is formed when an electron is transferred from the antioxidant molecule to the radical at an energy cost of IP. For both [$Cu_{P1}{}^{+}$−(T-OXY)$^{-2}_{dep}$]$^{-}$ and [Cu^{+}−2(T-OXY)$^{-2}_{dep}$]$^{-3}$ complexes, the IP energy is less than the PDE energy needed for the second step. This suggests that the second step is significantly more slow. Thus, the SET-PT process requires abundant energy and is highly improbable. On the other hand, the first step of SPLET is the slowest according to PA values. ArO^{-} anion formation requires energies much more significant than ETE, the energy needed to transfer an electron. This two-step mechanism requires a considerable energy. So, SPLET is unlikely to occur. Assessment of antioxidant property descriptors reaffirms that the two compounds of interest favor the HAT mechanism over SET-PT and SPLET in terms of energy, especially in the DMSO solvent. This preference aligns with the proposition that HAT is a pivotal process in human biology.[50] Although HAT and BDE($E0$) are two techniques with different respective formulas, both express the amount of energy required for

https://doi.org/10.1021/acsomega.3c07885
ACS Omega 2024, 9, 9076−9089

Table 3. Bond Lengths (Å) and Bond Angles (deg) for the Target Complexes Optimized at the PW91/TZP Level of Theory in DMSO

compounds	bond distances								bond angles	
	C_1–Cu	C_2–Cu	C_3–Cu	C_4–Cu	O_1–H_1	O_2–H_2	O_3–H_3	O_4–H_4	O_5–H_5	O_6–H_6	O_7–H_7	O_8–H_8	$\alpha(C_1CuC_2)$	$\theta(C_2CuC_3)$
Cu^+ Complexes														
$[Cu^+–2(T\text{-}OXY)]^+$	2.066	2.063	2.045	2.068	0.982	0.978	0.981	0.983	1.003	0.981	0.981	0.980	39.6	177.9
$[Cu^+–2(T\text{-}OXY)^{-2}_{dep}]^{-3}$	2.060	1.953	1.979	2.066	0.979	1.003	1.011	0.979	0.999	0.980	0.979	0.983	81.7	175.4
Cu^{2+} Complexes														
$[Cu^{2+}–2(T\text{-}OXY)]^{2+}$	2.079	2.095	2.095	2.167	0.982	0.980	0.984	0.981	0.979	0.983	0.982	0.981	40.5	172.4
$[Cu^{2+}–2(T\text{-}OXY)^{-2}_{dep}]^{-2}$	2.038	2.009	1.966	2.060	0.976	1.004	1.022	0.979	0.986	0.979	0.981	0.980	84.3	164.4

breakage of the OH bond and the departure of the dihydrogen atom for the free radical. To simplify our calculations, we advocate using BDE(*E*0) to determine the energy of homolytic O–H bond fragmentation since this technique is not restrictive regarding time and materials and has proven its effectiveness in several previous studies.[7,42]

4.3. Fragmentation by BDE(*E*0) of the O–H Bonds. The parameter BDE (E0) approach was obtained by a "single-point" calculation with PW91/TZP on the optimized structures. Every molecule is divided into two regions: the first is $[Cu\text{-}ArO]^{\bullet}$ and the atom of H is the second one. The COSMO model determined the decomposition energy results in DMSO (Table 5). Table 5 shows that the antioxidant activities of *cis*- and T-OXY are significantly affected by their complexation with Cu^+ and Cu^{2+}. According to BDE(E0), we found that all of the complexes had much higher antioxidant potential than Vitamin C, with BDE(E0) at 103.33 kcal/mol, and T-OXY, the highest antioxidant, at 121.89 kcal/mol.[7] Except for $[Cu_{P1}{}^{2+}–(T\text{-}OXY)]^{2+\prime}$ complexed via the ring carbon and $[Cu^{2+}–(C\text{-}OXY)]^{2+}$. This enhancement in antioxidant activity consistently favors cycle (B) of the molecular framework. The proximity of the copper ion to the prime antioxidant activity site enables efficient bond breaking. Consequently, the complexation of T-OXY at critical point 1 (BCP1) yields the most potent antiradical activity, either for Cu^+ or Cu^{2+}. Cu^+ complexes, characterized by both cis and trans geometries and present at all respective critical points, consistently exhibit superior antioxidant activity compared to T-OXY. This pattern is not mirrored in Cu^{2+} complexes. Based on the obtained BDE(E0) energy, the sequence of antiradical activity among the studied compounds follows:

$$
\begin{aligned}
[Cu^{+}_{P1}\text{-}(T\text{-}OXY)^{-2}_{dep}]^{-} &> [Cu^{+}_{P1}\text{-}(T\text{-}OXY)]^{+} \\
&> [Cu^{2+}_{P1}\text{-}(T\text{-}OXY)^{-2}_{dep}] \\
&> [Cu^{2+}_{P1}\text{-}(T\text{-}OXY)]^{2+} \\
&> [Cu^{+}_{P1}\text{-}(T\text{-}OXY)]^{+\prime} \\
&> [Cu^{+}\text{-}(C\text{-}OXY)^{-2}_{dep}]^{-} \\
&> [Cu^{+}\text{-}(C\text{-}OXY)]^{+} \\
&> [Cu^{+}_{P2}\text{-}(T\text{-}OXY)^{-2}_{dep}]^{-} \\
&> [Cu^{+}_{P2}\text{-}(T\text{-}OXY)]^{+} \\
&> [Cu^{2+}\text{-}(C\text{-}OXY)^{-2}_{dep}] \\
&> [Cu^{2+}_{P2}\text{-}(T\text{-}OXY)]^{2+} \\
&> [Cu^{2+}_{P2}\text{-}(T\text{-}OXY)^{-2}_{dep}] > T\text{-}OXY > [Cu^{2+}_{P1}\text{-}(T\text{-}OXY)]^{2+\prime} \\
&> [Cu^{2+}\text{-}(C\text{-}OXY)]^{2+}
\end{aligned}
$$

Notably, the complexes $[Cu_{P1}{}^{+}–(T\text{-}OXY)^{-2}_{dep}]^{-}$ and $[Cu_{P1}{}^{2+}–(T\text{-}OXY)^{-2}_{dep}]$ showcase optimal antioxidant activity within Cu^+ and Cu^{2+} complexes, respectively. Among these, $[Cu_{P1}{}^{+}–(T\text{-}OXY)^{-2}_{dep}]^{-}$ stands out with the strongest antioxidant activity, featuring a BDE(E0) value of 91.47 kcal/mol, the lowest within the study. A substantial discrepancy of 30.42 kcal/mol in DMSO is observed between $[Cu_{P1}{}^{+}–(T\text{-}OXY)^{-2}_{dep}]^{-}$ and T-OXY. Conversely, $[Cu_{P1}{}^{2+}–(T\text{-}OXY)^{-2}_{dep}]$ exhibits three sites with superior antioxidant activity than T-OXY. The antioxidant

https://doi.org/10.1021/acsomega.3c07885
ACS Omega 2024, 9, 9076–9089

Table 4. O−H Antioxidant Property Descriptors [kcal/mol] in DMSO at 298.15 K

	HAT	SET-PT		SPLET	
compound	BDE	IP	PDE	PA	ETE
$[Cu_{P1}^{+}-(T\text{-}OXY)_{dep}^{-2}]^{-}$ 5′-OH	64.13	219.46	442.37	485.84	175.97
$[Cu^{+}-2(T\text{-}OXY)_{dep}^{-2}]^{-3}$ 4-OH	29.23	166.89	273.46	344.45	95.90

Table 5. Analysis of the OH Bond Homolytic Dissociation Energy of Simple Bonded Molecules in DMSO at 298.15 K

		BDE(*E*0)				ref
compounds	OH	2-OH	4-OH	3′-OH	5′-OH	
T-OXY		130.87	129.83	121.89	122.16	7
ascorbic acid	103. 33					
		Cu^{+} Complexes				
$[Cu_{P1}^{+}-(T\text{-}OXY)]^{+}$		145.32	156.76	123.09	92.12	
$[Cu_{P1}^{+}-(T\text{-}OXY)]^{+\prime}$		106.16	123.54	135.97	101.54	
$[Cu_{P2}^{+}-(T\text{-}OXY)]^{+}$		145.08	145.00	116.20	105.80	
$[Cu^{+}-(C\text{-}OXY)]^{+}$		119.42	129.76	133.45	115.39	
$[Cu_{P1}^{+}-(T\text{-}OXY)_{dep}^{-2}]^{-}$		119.61	128.90	93.62	91.47	
$[Cu_{P2}^{+}-(T\text{-}OXY)_{dep}^{-2}]^{-}$		130.11	122.73	119.06	106.13	
$[Cu^{+}-(C\text{-}OXY)_{dep}^{-2}]^{-}$		127.03	113.33	115.18	102.08	
		Cu^{2+} Complexes				
$[Cu_{P1}^{2+}-(T\text{-}OXY)]^{2+}$		151.76	165.43	126.84	100.04	
$[Cu_{P1}^{2+}-(T\text{-}OXY)]^{2+\prime}$		129.68	158.84	132.93	127.19	
$[Cu_{P2}^{2+}-(T\text{-}OXY)]^{2+}$		152.37	169.86	124.87	119.46	
$[Cu^{2+}-(C\text{-}OXY)]^{2+}$		155.64	172.24	206.49	131.98	
$[Cu_{P1}^{2+}-(T\text{-}OXY)_{dep}^{-2}]$		127.64	133.16	116.20	94.57	
$[Cu_{P2}^{2+}-(T\text{-}OXY)_{dep}^{-2}]$		140.55	138.46	123.93	120.36	
$[Cu^{2+}-(C\text{-}OXY)_{dep}^{-2}]$		136.82	122.09	118.18	116.47	

Table 6. Analysis of the OH Bond Homolytic Dissociation Energy of Double-Bonded Molecules in DMSO at 298.15 K

	BDE(*E*0)							
compounds	H1	H2	H3	H4	H5	H6	H7	H8
				Cu^{+} Complexes				
$[Cu^{+}-2(T\text{-}OXY)]^{+}$	105.6	136.22	103.65	103.38	117.88	132.5	102.16	103.53
$[Cu^{+}-2(T\text{-}OXY)_{dep}^{-2}]^{-3}$	42.02	67.77	60.91	31.12	56.58	41.74	39.93	43.24
				Cu^{2+} Complexes				
$[Cu^{2+}-2(T\text{-}OXY)]^{2+}$	170.13	135.49	119.9	155.80	156.50	184.06	115.64	114.53
$[Cu^{2+}-2(T\text{-}OXY)_{dep}^{-2}]^{-2}$	68.94	87.88	79.14	59.24	80.06	72.68	67.21	69.03

activity order among the four sites of $[Cu_{P1}^{+}-(T\text{-}OXY)_{dep}^{-2}]^{-}$ follows:

$$5'\text{-OH} < 3'\text{-OH} < 2\text{-OH} < 4\text{-OH}$$

Consequently, the hydroxylation site's precise position in Resveratrol at 5′ is determined as the most potent antioxidant site across all complexes. Furthermore, it is noted that antioxidant activity is influenced by the dihedral angle $\theta(C_7C_1C_6C_8)$. A lower θ angle corresponds to higher antioxidant activity. This principle holds particularly true for the two complexes $[Cu_{P1}^{+}-(T\text{-}OXY)_{dep}^{-2}]^{-}$ and $[Cu_{P1}^{2+}-(T\text{-}OXY)_{dep}^{-2}]$, established as prime antioxidants.

Referring to the outcomes in Table 6, the complex with optimal antioxidant activity is $[Cu^{+}-2(T\text{-}OXY)_{dep}^{-2}]^{-3}$. H4 is the most robust site, featuring eight antioxidant sites, with an activity value of 31.12 kcal/mol. This signifies a 3.91-fold enhancement compared to T-OXY's activity at 121.89 kcal/mol. $[Cu^{2+}-2(T\text{-}OXY)_{dep}^{-2}]^{-2}$ follows, with its best site, with 59.24 kcal/mol, displaying an improved activity of 2.05 times compared to T-OXY.

Furthermore, outcomes from Tables 3 and 7 indicate distinguishable O−H bond lengths, and charge distribution reveals polarized bonds in $[Cu^{+}-2(T\text{-}OXY)]^{+}$ and $[Cu^{+}-2(T\text{-}OXY)_{dep}^{-2}]^{-3}$.

Remarkably, all homolytic O−H bond fragmentations exhibit values with substantial differences between chelated and deprotonated complexes. Earlier experimental research demonstrated that enhanced ligand basicity correlates with heightened antioxidant activity, surpassing L-ascorbic acid.[51] In our study, the structure yielding the most favorable antioxidant results across all analyses is the anionic complex containing the basic ligand (−4 hydrogens), $[Cu^{+}-2(T\text{-}OXY)_{dep}^{-2}]^{-3}$. This trend also holds for $[Cu^{2+}-2(T\text{-}OXY)_{dep}^{-2}]^{-2}$. Notably, hydrogen detachment in the $[Cu^{+}-2(T\text{-}OXY)_{dep}^{-2}]^{-3}$ complex proves easier than in the $[Cu^{2+}-2(T\text{-}OXY)_{dep}^{-2}]^{-2}$ complex. Consequently, antioxidant activity can be ranked as follows: $[Cu^{+}-2(T\text{-}OXY)_{dep}^{-2}]^{-3}$ > $[Cu^{2+}-2(T\text{-}OXY)_{dep}^{-2}]^{-2}$ > $[Cu^{+}-2(T\text{-}OXY)]^{+}$ > $[Cu^{2+}-2(T\text{-}OXY)]^{2+}$ > T-OXY. To summarize, the top-performing antioxidant complexes are ranked as follows: $[Cu^{+}-2(T\text{-}OXY)_{dep}^{-2}]^{-3}$ > $[Cu_{P1}^{+}-(T\text{-}OXY)_{dep}^{-2}]^{-}$ > T-OXY.

4.4. Electronic Properties. The electronic characteristics of compounds tell us a lot about their antioxidant activity.

https://doi.org/10.1021/acsomega.3c07885
ACS Omega 2024, 9, 9076−9089

Table 7. Hirshfeld Charges of the H and O of the Cu^+ Complexes: $[Cu^+-2(T\text{-}OXY)]^+$ Chelated and $[Cu^+-2(T\text{-}OXY)^{-2}_{dep}]^{-3}$ Deprotonated

compounds	H1		H2		H3		H4		H5		H6		H7		H8	
	O	H	O	H	O	H	O	H	O	H	O	H	O	H	O	H
$[Cu^+-2(T\text{-}OXY)]^+$	−0.120	0.219	−0.178	0.202	−0.144	0.209	−0.151	0.212	−0.216	0.106	−0.186	0.199	−0.142	0.213	−0.152	0.201
$[Cu^+-2(T\text{-}OXY)^{-2}_{dep}]^{-3}$	−0.229	0.176	−0.240	0.087	−0.220	0.076	−0.219	0.184	−0.241	0.117	−0.223	0.179	−0.219	0.176	−0.243	0.142

Therefore, exploiting these properties is crucial to understanding their antioxidant behaviors (see Table 8).

Analyzing Table 8 reveals that the complexation of ligands C- and T-OXY with Cu^+ in Bond Critical Points (BCP1) and (2) exhibits more excellent stability than complexes involving Cu^{2+}, respectively. However, complexes of neutral ligands with Cu^+ and Cu^{2+} at (BCP2) demonstrate higher stability than their counterparts at (BCP1). This trend is reversed for deprotonated, negatively charged ligands (−2). Contrary to intuitive chemical expectations, the complex energies demonstrate that binding copper ions with isolated oxygen pairs is energetically unfavorable. Instead, copper ions preferentially bind to carbon atoms. The most stable structures involve bonds and interactions between the copper atom and carbon atoms within the aromatic ring and the C═C double bond. Surprisingly, our study indicates that metallic bonds interact more with the π electrons of the OXY backbone than with isolated oxygen pairs. This phenomenon parallels the process of copper coordination with Resveratrol, which was discovered experimentally and theoretically in studies.[26,27]

The energy gaps calculated for copper complexes are higher than 1.5 eV, indicating strong stability.[52] Unlike other cis complexes, $[Cu^+-(C\text{-}OXY)]^+$ and $[Cu^{2+}-(C\text{-}OXY)]^{2+}$ contribute to their lower reactivity in comparison to other complexes' antioxidant activity.[53] The complex $[Cu_{P1}{}^+-(T\text{-}OXY)^{-2}_{dep}]^-$ exhibits the highest HOMO energy, underscoring its role as an excellent electron donor in electron transfer reactions. Therefore, complexation at (BCP1) results in complexes with superior antiradical activity. A similar trend is observed in the complex $[Cu_{P1}{}^{2+}-(T\text{-}OXY)^{-2}_{dep}]$, reinforcing the results from BDE(*E*0) fragmentation analysis.

Values of the Hirshfeld charges are summarized in Tables 7 and 8. These charges highlight a significant shift in the distribution of charges on Cu^+ and Cu^{2+} as they transition from their free states (1+ and 2+) to those coordinated with neutral or deprotonated ligands. Cu^+ and Cu^{2+} maintain their positive charges, but there is an apparent increase in negative charges on the latter. The difference in charges between free and bound Cu in extreme compounds (Cu 0.50) and (Cu 0.13) with a single ligand and (Cu 0.20) and (Cu 0.20) for two ligands aligns with the covalent contribution in the metal−ligand bond (covalent bond).

Regarding the outcomes summarized in Table 9, it is evident that the complexes involving two deprotonated ligands with metal ions Cu^{2+} and Cu^+ denoted as $[Cu^{2+}-2(T\text{-}OXY)^{-2}_{dep}]^{-2}$ and $[Cu^+-2(T\text{-}OXY)^{-2}_{dep}]^{-3}$, respectively, are less stable compared to complexes formed by the two saturated OXY ligands $[Cu^+-2(T\text{-}OXY)]^+$ and $[Cu^{2+}-2(T\text{-}OXY)]^{2+}$.

The complex with the best antioxidant activity is $[Cu^+-2(T\text{-}OXY)^{-2}_{dep}]^{-3}$, which goes in the opposite direction of stability. It has the highest HOMO and the lowest *E*(gap), thus proving that it is the best electron donor among the four complexes with two ligands. Consequently, they possess the highest antioxidant activity. Among the one-ligand series, the complex $[Cu_{P1}{}^+-(T\text{-}OXY)^{-2}_{dep}]^-$ and in the two-ligand series, $[Cu^+-2(T\text{-}OXY)^{-2}_{dep}]^{-3}$ exhibit the strongest antiradical activity among all of the studied complexes, as they can more readily donate an electron.

4.5. Orbital Analysis. The graphic representations of the orbitals of the complexes of Cu^+ and Cu^{2+} with one or two ligands by the DFT/PW91/TZP/DMSO method are represented in Figure 6 for the two series of Cu^+ and Cu^{2+} complexes with one or two ligands; the existence of a covalent

https://doi.org/10.1021/acsomega.3c07885
ACS Omega 2024, 9, 9076−9089

Table 8. Energy of Optimization E (eV), HOMO (eV), E(gap) (eV), and Cu^{+}/Cu^{2+} Hirshfeld Charge for the Target Complexes Calculated at DFT PW91/TZP in DMSO Solvent at 298.15 K

compounds	E (eV)	HOMO (eV)	E(gap) (eV)	Hirshfeld charge	
		Cu^{+} Complexes			
$[Cu_{P1}{}^{+}-(T\text{-}OXY)]^{+}$	−189.09	−4.13	2.28	Cu^{+}: 0.40	O: −0.10
$[Cu_{P1}{}^{+}-(T\text{-}OXY)]^{+\prime}$	−189.06	−3.61	2.45	Cu^{+}: 0.45	C: −0.12
$[Cu_{P2}{}^{+}-(T\text{-}OXY)]^{+}$	−189.40	−4.20	2.62	Cu^{+}: 0.50	C: −0.08
$[Cu^{+}-(C\text{-}OXY)]^{+}$	−189.48	−3.61	2.75	Cu^{+}: 0.40	C: −0.06. C: −0.12
$[Cu_{P1}{}^{+}-(T\text{-}OXY)_{dep}^{-2}]^{-}$	−189.07	−2.12	1.99	Cu^{+}: 0.15	C: −0.23. C: −0.21
$[Cu_{P2}{}^{+}-(T\text{-}OXY)_{dep}^{-2}]^{-}$	−188.96	−2.13	2.28	Cu^{+}: 0.14	C: −0.21. C: −0.20
$[Cu^{+}-(C\text{-}OXY)_{dep}^{-2}]^{-}$	−189.39	−2.13	2.19	Cu^{+}: 0.13	C: −0.22. C: −0.20
		Cu^{2+} Complexes			
$[Cu_{P1}{}^{2+}-(T\text{-}OXY)]^{2+}$	−183.89	−6.35	2.28	Cu^{2+}: 0.70	O: −0.07
$[Cu_{P1}{}^{2+}-(T\text{-}OXY)]^{2+\prime}$	−184.27	−6.42	2.56	Cu^{2+}: 0.60	C: −0.10
$[Cu_{P2}{}^{2+}-(T\text{-}OXY)]^{2+}$	−184.82	−6.28	2.27	Cu^{2+}: 0.70	C: −0.04. C: −0.05
$[Cu^{2+}-(C\text{-}OXY)]^{2+}$	−184.62	−6.44	2.77	Cu^{2+}: 0.50	C: −0.05. C: −0.10
$[Cu_{P1}{}^{2+}-(T\text{-}OXY)_{dep}^{-2}]$	−186.24	−4.26	2.23	Cu^{2+}: 0.30	C:-0.12. C: −0.12
$[Cu_{P2}{}^{2+}-(T\text{-}OXY)_{dep}^{-2}]$	−185.96	−4.71	2.28	Cu^{2+}: 0.40	C: −0.13. C: −0.13
$[Cu^{2+}-(C\text{-}OXY)_{dep}^{-2}]$	−185.92	−5.10	2.64	Cu^{2+}: 0.35	C: −0.17. C: −0.12

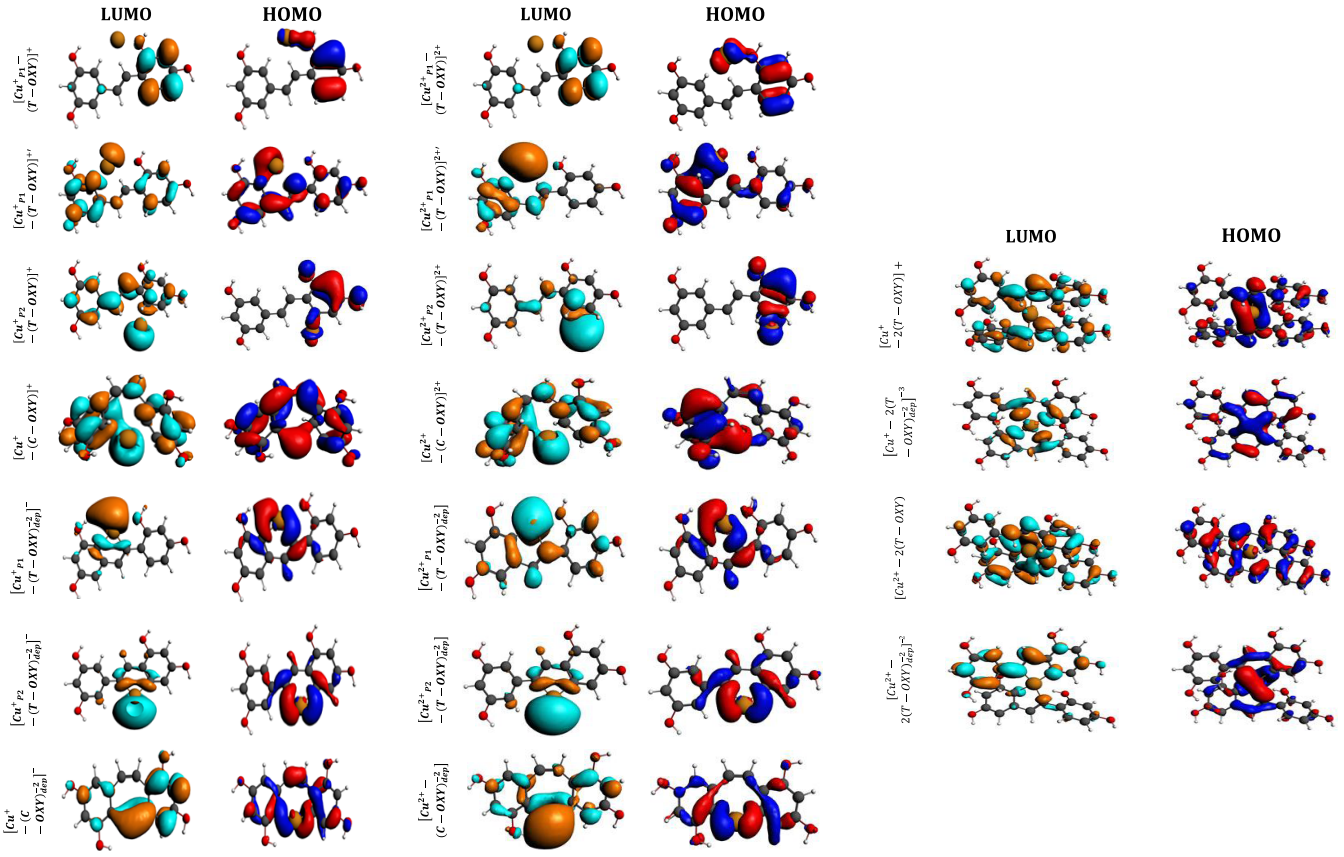

Figure 6. Graphical representation of HOMOs and LUMOs of Cu^{+} and Cu^{2+} complexes, respectively, by the PW91/TZP/DMSO level of theory.

bond is observed in view of the frontier orbitals' nodal properties. This is consistent with the covalent contribution found in the fragmentation of metal−ligand bonds.

4.6. Description of Bonds in Cu Ligand. *4.6.1. Coordination Bond Decomposition Energy (BDE) Analysis.* An analysis aimed to quantify the degree of ionic and covalent bonding within metal−ligand bonds in copper complexes using energy decomposition, as in eq 7.[54] This investigation is important as it sheds light on bonding characteristics with the antioxidant activity of these complexes. Indeed, hydrogen loss and the formation of stable radicals represent pivotal steps in antiradical activity. Thus, knowing the energy decomposition becomes pertinent to unravel its role in stabilizing radical forms and consequently influencing antioxidant activity. Based on the Ziegler−Rauk energy diagram decomposition.[55] The complex's negatively charged or optimized neutral ligands are introduced as a single fragment. Subsequently, their interaction with the metal center is studied. This binding energy of a complex is the sum of three terms:

$$\mathrm{BDE} = E_{\mathrm{elect}} + E_{\mathrm{Pauli}} + E_{\mathrm{orb}} \quad (7)$$

The results of the BDE are shown in Figures 7, 8, and 9.

https://doi.org/10.1021/acsomega.3c07885
ACS Omega 2024, 9, 9076−9089

Table 9. Energy of Optimization *E* (eV), HOMO (eV), *E*(gap) (eV), and Cu^{+}/Cu^{2+} Hirshfeld Charge for the Target Complexes with Bi-2,4,3′,5′-Tetrahydroxystilbene Neutral and Deprotonated Calculated at the DFT PW91/TZP/DMSO Level of Theory at 298.15 K

compounds	*E* (eV)	HOMO (eV)	*E*(gap) (eV)	Hirshfeld charge	
			Cu^{+} Complexes		
$[Cu^{+}-2(T\text{-}OXY)]^{+}$	−384.12	−3.88	2.6	Cu^{+}: 0.40	C1: −0.08. C2: −0.05. C3: −0.08. C4: −0.08
$[Cu^{+}-2(T\text{-}OXY)^{-2}_{dep}]^{-3}$	−378.75	−1.57	0.6	Cu^{+}: 0.20	C1: −0.06. C2: −0.17. C3: −0.19. C4: −0.21
			Cu^{2+} Complexes		
$[Cu^{2+}-2(T\text{-}OXY)]^{2+}$	−379.28	−5.54	2.03	Cu^{2+}: 0.45	C1: −0.06. C2: −0.02. C3: −0.05. C4: −0.03
$[Cu^{2+}-2(T\text{-}OXY)^{-2}_{dep}]^{-2}$	−377.60	−2.48	2.18	Cu^{2+}: 0.20	C1: −0.17. C2: −0.18. C3: −0.19. C4: −0.16

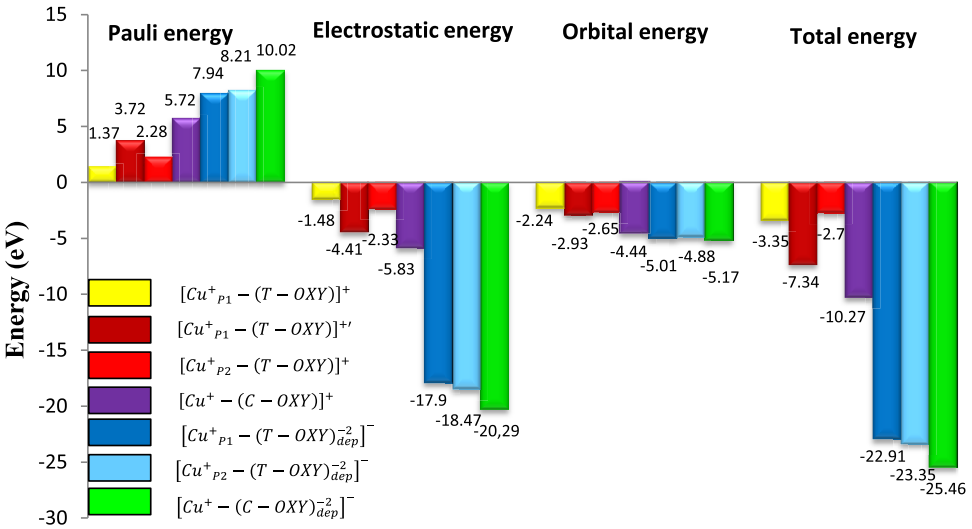

Figure 7. Graphic representation of various energy contributions of Cu^{+} complexes.

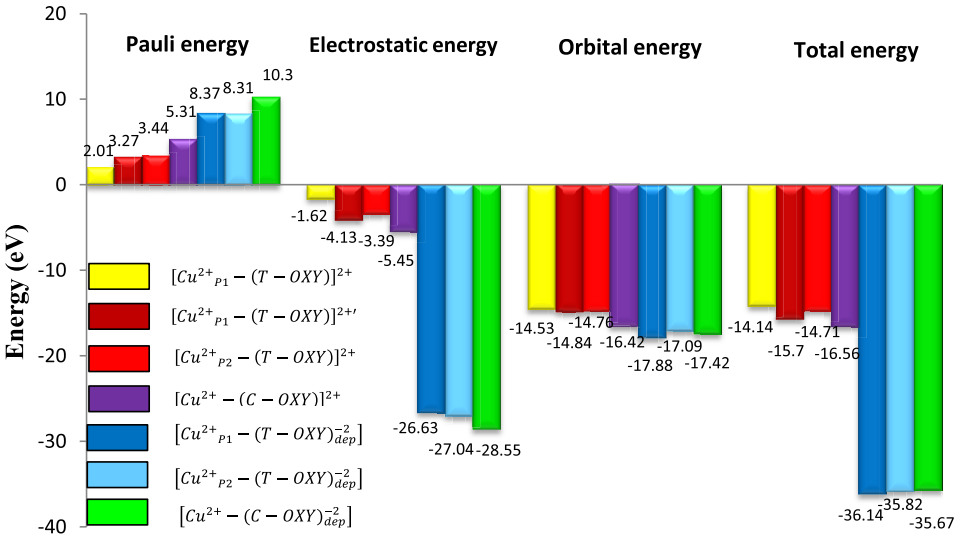

Figure 8. Graphic representation of various energy contributions of Cu^{2+} complexes.

The degree of covalence in the metal−ligand bond can be measured by the electrostatic and orbital energies ratio.[54] The calculations were carried out without destabilizing energies and considering purely ionic and covalent bonds. Tables 10 and 11 summarize the results of the BDE achieved. They show that the electrostatic contributions dominate all Cu^{+} complexes with one or two neutral or deprotonated ligands. This corroborates the analysis of figures for Cu^{2+}-*trans* or -*cis* OXY complexes where the percentage of E_{elect} and E_{orb} confirms the predominance of the attractive orbital interaction. These results support the analysis of Figures 7 and 8 (by omitting Pauli's destabilization).

5. CONCLUSIONS

An in-depth comparative exploration was conducted using density functional theory (DFT) to assess the antioxidant properties of 18 stable exhaustive complexes involving Cu^{+} and Cu^{2+} ions. These complexes included neutral and deprotonated forms of T-OXY and C-OXY ligands, each with one or two

https://doi.org/10.1021/acsomega.3c07885
ACS Omega 2024, 9, 9076−9089

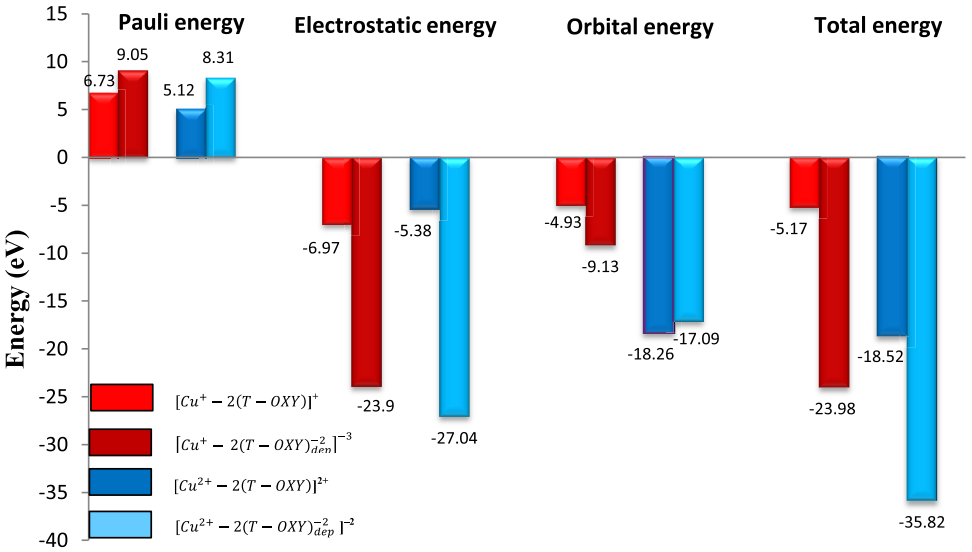

Figure 9. Graphic representation of various energy contributions of Cu^{+} and Cu^{2+} complexes.

Table 10. Percentage of Electrostatic and Orbital Contributions of Cu^{+} and Cu^{2+} Complexes with Mono-2,4,3′,5′-tetrahydroxystilbene Neutral and Deprotonated in DMSO

compounds	% E_{orb}	% E_{elect}
Cu^{+} Complexes		
$[Cu_{P1}{}^{+}-(T\text{-}OXY)]^{+}$	60.00	40.00
$[Cu_{P1}{}^{+}-(T\text{-}OXY)]^{+\prime}$	40.00	60.00
$[Cu_{P2}{}^{+}-(T\text{-}OXY)]^{+}$	53.00	47.00
$[Cu^{+}-(C\text{-}OXY)]^{+}$	43.00	57.00
$[Cu_{P1}{}^{+}-(T\text{-}OXY)^{-2}_{dep}]^{-}$	22.00	78.00
$[Cu_{P2}{}^{+}-(T\text{-}OXY)^{-2}_{dep}]^{-}$	21.00	79.00
$[Cu^{+}-(C\text{-}OXY)^{-2}_{dep}]^{-}$	20.00	80.00
Cu^{2+} Complexes		
$[Cu_{P1}{}^{2+}-(T\text{-}OXY)]^{2+}$	90.00	10.00
$[Cu_{P1}{}^{2+}-(T\text{-}OXY)]^{2+\prime}$	78.00	22.00
$[Cu_{P2}{}^{2+}-(T\text{-}OXY)]^{2+}$	81.00	19.00
$[Cu^{2+}-(C\text{-}OXY)]^{2+}$	75.00	25.00
$[Cu_{P1}{}^{2+}-(T\text{-}OXY)^{-2}_{dep}]$	40.00	60.00
$[Cu_{P2}{}^{2+}-(T\text{-}OXY)^{-2}_{dep}]$	39.00	61.00
$[Cu^{2+}-(C\text{-}OXY)^{-2}_{dep}]$	38.00	62.00

Table 11. Percentage of Electrostatic and Orbital Contributions of Cu^{+} and Cu^{2+} Complexes with Bi-2,4,3′,5′-tetrahydroxystilbene Neutral and Deprotonated in DMSO

compounds	% E_{orb}	% E_{elect}
Cu^{+} Complexes		
$[Cu^{+}-2(T\text{-}OXY)]^{+}$	41.00	59.00
$[Cu^{+}-2(T\text{-}OXY)^{-2}_{dep}]^{-3}$	28.00	72.00
Cu^{2+} Complexes		
$[Cu^{2+}-2(T\text{-}OXY)]^{2+}$	77.00	23.00
$[Cu^{2+}-2(T\text{-}OXY)^{-2}_{dep}]^{-2}$	40.00	60.00

ligands. The study carried out the main mechanisms of antioxidant activity: BDE(*E*0) to quantify the homolytic decomposition energies of O−H, HAT, SET-PT, and SPLET. Their structural and electronic studies were provided in the presence of the solvent DMSO.

The antioxidant descriptors, BDE, IP, PDE, PA, and ETE, indicated that the HAT mechanism is the best for the remaining SET-PT and SPLET in energy terms. Notably, all of the complexes with Cu^{+} with both cis and trans geometries on all of the respective critical points possess higher antioxidant activity than T-OXY, which is not the case for the Cu^{2+} ion. Notably, the complexation at the critical point P1 gives complexes with excellent antiradical properties, attributed to the supplementary metallic bond's O−H bond polarization.

Among the findings, complexes denoted as $[Cu_{P1}{}^{+}-(T\text{-}OXY)^{-2}_{dep}]^{-}$ and $[Cu^{+}-2(T\text{-}OXY)^{-2}_{dep}]^{-3}$, derived from deprotonation, demonstrated exceptional antioxidant performance. These complexes possessed the highest HOMO orbital energy and the lowest HOMO−LUMO energy gap, showcasing their efficacy as electron donors. The electrostatic contributions dominate all Cu^{+} complexes with one or two ligands. Nevertheless, for the Cu^{2+} complexes, the orbital contribution is the majority. The nodal properties of the frontier orbitals of the 18 complexes clearly show the existence of a covalent bond. This is consistent with the strong orbital energy contribution found in the fragmentation of the metal−ligand bonds.

The complexes denoted as $[Cu^{2+}-2(T\text{-}OXY)]^{2+}$ and $[Cu^{+}-2(T\text{-}OXY)]^{+}$, both comprising two ligands, adopt a square-based pyramidal geometry. In contrast, anionic complexes $[Cu^{2+}-2(T\text{-}OXY)^{-2}_{dep}]^{-2}$ and $[Cu^{+}-2(T\text{-}OXY)^{-2}_{dep}]^{-3}$ adopt a pseudo-square planar geometry. The latter two complexes demonstrated the highest antioxidant potency. Our results show that the deprotonation of the ligands increased their basicity, stimulating the antioxidant activity.[51] Notably, among the 18 explored complexes, $[Cu_{P1}{}^{+}-(T\text{-}OXY)^{-2}_{dep}]^{-}$ and $[Cu^{+}-2(T\text{-}OXY)^{-2}_{dep}]^{-3}$ emerged as the most promising antioxidant candidates, surpassing T-OXY by a factor of 3.91 and even surpassing the antioxidant efficiency of Vitamin C. These results advocate for their synthesis in future applications within the pharmaceutical and food industries based on the conducted calculations.

Our investigation confirms that the process of direct chelation or coupled chelation-deprotonation, as well as the metal's charge and especially the ligands' basicity, significantly impacts the antioxidant activity of polyphenolic compounds.

https://doi.org/10.1021/acsomega.3c07885
ACS Omega 2024, 9, 9076−9089

AUTHOR INFORMATION

Corresponding Author

Yacine Benguerba − *Laboratoire de Biopharmacie and Pharmacotechnie (LBPt), Department of Process Engineering, Faculty of Technology, Ferhat Abbas Setif 1 University, 19000 Setif, Algeria;* orcid.org/0000-0002-8251-9724; Email: yacinebenguerba@univ-setif.dz

Authors

Salima Hamadouche − *Laboratoire de Chimie des Matériaux et des Vivants: Activité & Réactivité (LCMVAR), Université Batna 1, 5000 Batna, Algeria*

Hafida Merouani − *Laboratoire de Chimie des Matériaux et des Vivants: Activité & Réactivité (LCMVAR), Université Batna 1, 5000 Batna, Algeria; Département de Socle Commun, Faculté de Technologie, Université Ben Boulaid Batna 2, 05078 Batna, Algeria*

Abd Alghani May − *Département de Chimie, Faculté des Sciences Exacte, Université Frères Mentouri 1, 25017 Constantine, Algeria*

Nadia Ouddai − *Laboratoire de Chimie des Matériaux et des Vivants: Activité & Réactivité (LCMVAR), Université Batna 1, 5000 Batna, Algeria*

Manawwer Alam − *Department of Chemistry, College of Science, King Saud University, Riyadh 11451, Saudi Arabia;* orcid.org/0000-0001-9540-8532

Luca Micoli − *Dipartimento di Ingegneria Chimica, dei Materiali e della Produzione Industriale, Università di Napoli Federico II, 80125 Napoli, Italy*

Alessandro Erto − *Dipartimento di Ingegneria Industriale, Università di Napoli Federico II, 80125 Napoli, Italy;* orcid.org/0000-0002-6956-7924

Complete contact information is available at: https://pubs.acs.org/10.1021/acsomega.3c07885

Notes

The authors declare no competing financial interest.

ACKNOWLEDGMENTS

The authors are thankful to the Researchers Supporting Project (RSP2024R113), King Saud University, Riyadh, Saudi Arabia.

REFERENCES

(1) Lorenz, P.; et al. Oxyresveratrol and Resveratrol are potent antioxidants and free radical scavengers: effect on nitrosative and oxidative stress derived from microglial cells. *Nitric Oxide* **2003**, *9* (2), 64−76, DOI: 10.1016/j.niox.2003.09.005.

(2) Likhitwitayawuid, K.; et al. Phenolics with antiviral activity from Millettia erythrocalyx and Artocarpus lakoocha. *Nat. Prod. Res.* **2005**, *19* (2), 177−182, DOI: 10.1080/14786410410001704813.

(3) Lyons, M. M.; et al. Resveratrol in raw and baked blueberries and bilberries. *J. Agric. Food Chem.* **2003**, *51* (20), 5867−5870, DOI: 10.1021/jf034150f.

(4) Chung, K.-O.; et al. In-vitro and in-vivo anti-inflammatory effect of oxyresveratrol from Morus alba L. *J. Pharm. Pharmacol.* **2010**, *55* (12), 1695−1700, DOI: 10.1211/0022357022313.

(5) Andrabi, S. A.; et al. Oxyresveratrol (trans-2, 3′, 4, 5′-tetrahydroxystilbene) is neuroprotective and inhibits the apoptotic cell death in transient cerebral ischemia. *Brain Res.* **2004**, *1017* (1−2), 98−107, DOI: 10.1016/j.brainres.2004.05.038.

(6) Qiu, F.; et al. Pharmacological properties of traditional medicines. XXII. Pharmacokinetic study of mulberroside A and its metabolites in rat. *Biol. Pharm. Bull.* **1996**, *19* (11), 1463−1467, DOI: 10.1248/bpb.19.1463.

(7) Hamadouche, S.; et al. Theoretical evaluation of the antioxidant activity of some stilbenes using the Density Functional Theory. *J. Mol. Struct.* **2021**, *1229*, No. 129496, DOI: 10.1016/j.molstruc.2020.129496.

(8) Kostyuk, V.; et al. influence of metal ions on flavonoid protection against asbestos-induced cell injury. *Arch. Biochem. Biophys.* **2001**, *385* (1), 129−137, DOI: 10.1006/abbi.2000.2118.

(9) Prajapati, R.; et al. Structural characterization and cytotoxicity studies of ruthenium (II)−dmso−chloro complexes of chalcone and flavone derivatives. *Polyhedron* **2010**, *29* (3), 1055−1061, DOI: 10.1016/j.poly.2009.11.012.

(10) Kasprzak, M. M.; Erxleben, A.; Ochocki, J. Properties and applications of flavonoid metal complexes. *RSC Adv.* **2015**, *5* (57), 45853−45877, DOI: 10.1039/c5ra05069c.

(11) Alsoliemy, A.; et al. synthesis, characterization and self-assembly of new cholesteryl-substitued sym-tetrazine: Fluorescence, gelation and mesogenic properties. *J. Mol. Liq.* **2021**, *342*, No. 117543, DOI: 10.1016/j.molliq.2021.117543.

(12) Ispir, E.; et al. Synthesis, structural characterization, electrochemical, photoluminescence, antiproliferative and antioxidant properties of Co (II), Cu (II) and Zn (II) complexes bearing the azo-azomethine ligands. *J. Mol. Struct.* **2019**, *1182*, 63−71, DOI: 10.1016/j.molstruc.2019.01.029.

(13) Mary, C. P. V.; et al. Metal chelating ability and antioxidant properties of Curcumin-metal complexes−A DFT approach. *J. Mol. Graphics Model.* **2018**, *79*, 1−14, DOI: 10.1016/j.jmgm.2017.10.022.

(14) Alzahrani, R.; et al. synthesis and characterization for new Mn (II) complexes; conductometry, DFT, antioxidant activity via enhancing superoxide dismutase enzymes that confirmed by in-silico and in-vitro ways. *J. Mol. Struct.* **2021**, *1243*, No. 130855, DOI: 10.1016/j.molstruc.2021.130855.

(15) Berthon, G. Is copper pro-or anti-inflammatory? A reconciling view and a novel approach for the use of copper in the control of inflammation. *Agents Actions* **1993**, *39*, 210−217, DOI: 10.1007/bf01998975.

(16) Galano, A.; Francisco Marquez, M.; Pérez-González, A. Ellagic acid: an unusually versatile protector against oxidative stress. *Chem. Res. Toxicol.* **2014**, *27* (5), 904−918, DOI: 10.1021/tx500065y.

(17) Alharbi, A.; et al. Green synthesis approach for new Schiff's-base complexes; theoretical and spectral based characterization with in-vitro and in-silico screening. *J. Mol. Liq.* **2022**, *345*, No. 117803, DOI: 10.1016/j.molliq.2021.117803.

(18) Alkhamis, K.; et al. Conductometry of nano-sized zinc sulfate; synthesis and characterization of new hydrazone complexes: conformational and in-vitro assay. *J. Mol. Liq.* **2021**, *340*, No. 117167, DOI: 10.1016/j.molliq.2021.117167.

(19) Al-Abdulkarim, H. A.; et al. Optimization for synthesized quinoline-based Cr3+, VO2+, Zn2+ and Pd2+ complexes: DNA interaction, biological assay and in-silico treatments for verification. *J. Mol. Liq.* **2021**, *339*, No. 116797, DOI: 10.1016/j.molliq.2021.116797.

(20) Ding, W. Q.; Lind, S. Metal ionophores−an emerging class of anticancer drugs. *IUBMB Life* **2009**, *61* (11), 1013−1018, DOI: 10.1002/iub.253.

(21) Saadeh, S. M. Synthesis, characterization and biological properties of Co (II), Ni (II), Cu (II) and Zn (II) complexes with an SNO functionalized ligand. *Arab. J. Chem.* **2013**, *6* (2), 191−196, DOI: 10.1016/j.arabjc.2010.10.002.

(22) Singh, K.; Barwa, M. S.; Tyagi, P. Synthesis, characterization and biological studies of Co (II), Ni (II), Cu (II) and Zn (II) complexes with bidentate Schiff bases derived by heterocyclic ketone. *Eur. J. Med. Chem.* **2006**, *41* (1), 147−153, DOI: 10.1016/j.ejmech.2005.06.006.

(23) Vedanayaki, S.; Jayaseelan, P. Synthesis, structural characterization and biological properties of Cu (II), Ni (II), Mn (II), Zn (II) and VO (II) complexes of tetradentate Schiff bases. *Eur. J. Chem.* **2016**, *7* (3), 368−374, DOI: 10.5155/eurjchem.7.3.368-374.1443.

(24) Ejidike, I. P.; Ajibade, P. Synthesis, characterization and biological studies of metal (II) complexes of (3 E)-3-[(2-{(E)-[1-(2, 4-dihydroxyphenyl) ethylidene] amino} ethyl) imino]-1-phenylbutan-1-one Schiff base. *Molecules* **2015**, *20* (6), 9788−9802, DOI: 10.3390/molecules20069788.
(25) Alper, P.; et al. synthesis, characterization, anticancer and antioxidant activity of new nickel (II) and copper (II) flavonoid complexes. *J. Mol. Struct.* **2019**, *1196*, 783−792, DOI: 10.1016/j.molstruc.2019.07.009.
(26) Tamboli, V.; et al. A study of resveratrol-copper complexes by electrospray ionization mass spectrometry and density functional theory calculations. *Rapid Commun. Mass Spectrom.* **2011**, *25* (4), 526−532, DOI: 10.1002/rcm.4883.
(27) Chiavarino, B.; et al. Infrared spectroscopy of copper-resveratrol complexes: A joint experimental and theoretical study. *J. Chem. Phys.* **2012**, *137* (2), No. 024307, DOI: 10.1063/1.4732583.
(28) Mayer, J. M.; Rhile, I. Thermodynamics and kinetics of proton-coupled electron transfer: stepwise vs. concerted pathways. *Biochim. Biophys. Acta* **2004**, *1655*, 51−58, DOI: 10.1016/j.bbabio.2003.07.002.
(29) Bâldea, I. Two Theorems and Important Insight on How the Preferred Mechanism of Free Radical Scavenging Cannot Be Settled. *Molecules* **2022**, *27* (22), No. 8092, DOI: 10.3390/molecules27228092.
(30) Di Meo, F.; et al. Free radical scavenging by natural polyphenols: Atom versus electron transfer. *J. Phys. Chem. A* **2013**, *117* (10), 2082−2092, DOI: 10.1021/jp3116319.
(31) Boerrigter, P.; et al. Three-dimensional numerical integration for electronic structure calculations. *Int. J. Quantum Chem.* **1988**, *33* (2), 87−113, DOI: 10.1002/qua.560330204.
(32) Te Velde, G.; et al. Chemistry with ADF. *J. Comput. Chem.* **2001**, *22* (9), 931−967.
(33) Aprà, E.; Fortunelli, A. Density-functional study of Pt13 and Pt55 cuboctahedral clusters. *J. Mol. Struct.: THEOCHEM* **2000**, *501*, 251−259.
(34) Versluis, L.; Ziegler, T. determination of molecular structures by density functional theory. The evaluation of analytical energy gradients by numerical integration. *J. Chem. Phys.* **1988**, *88* (1), 322−328, DOI: 10.1063/1.454603.
(35) Pye, C. C.; Ziegler, T. An implementation of the conductor-like screening model of solvation within the Amsterdam density functional package. *Theor. Chem. Acc.* **1999**, *101* (6), 396−408.
(36) Ounissi, A.; et al. Theoretical investigation on structural and physicochemical properties of some ionic liquids. *Comput. Theor. Chem.* **2016**, *1092*, 68−73, DOI: 10.1016/j.comptc.2016.08.007.
(37) Pye, C. C.; Ziegler, T. An implementation of the conductor-like screening model of solvation within the Amsterdam density functional package. *Can. J. Chem.* **1999**, *101*, 396−408, DOI: 10.1139/v09-008.
(38) Rimarčík, J.; et al. study of the solvent effect on the enthalpies of homolytic and heterolytic N−H bond cleavage in p-phenylenediamine and tetracyano-p-phenylenediamine. *J. Mol. Struct.: THEOCHEM* **2010**, *952* (1−3), 25−30, DOI: 10.1016/j.theochem.2010.04.002.
(39) Cao, H.; et al. Density functional theory calculations for Resveratrol. *Bioorg. Med. Chem. Lett.* **2003**, *13* (11), 1869−1871, DOI: 10.1016/S0960-894X(03)00283-X.
(40) Caruso, F.; et al. Structural basis for antioxidant activity of trans-resveratrol: ab initio calculations and crystal and molecular structure. *J. Agric. Food Chem.* **2004**, *52* (24), 7279−7285, DOI: 10.1021/jf048794e.
(41) Boussebbat, W.; et al. Theoretical aspect of the bonding in bis-chelate thiosemicarbazones nickel (II) complexes: A DFT study. *J. Mol. Struct.* **2018**, *1154*, 19−26, DOI: 10.1016/j.molstruc.2017.09.062.
(42) Baira, K.; et al. Multitask Quantum Study of the Curcumin-Based Complex Physicochemical and Biological Properties. *Int. J. Mol. Sci.* **2022**, *23* (5), 2832 DOI: 10.3390/ijms23052832.
(43) Lakehal, S.; Ouddai, N.; Bououdina, M. Theoretical investigation on homoleptic Yttrium tri-guanidinates. *Arab. J. Chem.* **2014**, *7* (6), 1124−1130, DOI: 10.1016/j.arabjc.2013.03.004.
(44) Villaño, D.; et al. Comparison of antioxidant activity of wine phenolic compounds and metabolites in vitro. *Anal. Chim. Acta* **2005**, *538* (1−2), 391−398, DOI: 10.1016/j.aca.2005.02.016.
(45) Mazzone, G.; et al. Antioxidant properties comparative study of natural hydroxycinnamic acids and structurally modified derivatives: Computational insights. *Comput. Theor. Chem.* **2016**, *1077*, 39−47, DOI: 10.1016/j.comptc.2015.10.011.
(46) Aourabi, S.; et al. Phenolic fraction of Ammi visnaga extract as environmentally friendly antioxidant and corrosion inhibitor for mild steel in acidic medium. *J. Mol. Liq.* **2021**, *323*, No. 114950, DOI: 10.1016/j.molliq.2020.114950.
(47) Leopoldini, M.; et al. Antioxidant properties of phenolic compounds: H-atom versus electron transfer mechanism. *J. Phys. Chem. A* **2004**, *108* (22), 4916−4922, DOI: 10.1021/jp037247d.
(48) Allen, F. H.; et al. Tables of bond lengths determined by X-ray and neutron diffraction. Part 1. Bond lengths in organic compounds. *J. Chem. Soc., Perkin Trans. 2* **1987**, No. 12, S1−S19, DOI: 10.1039/p298700000s1.
(49) Chen, Y.; et al. Structure-thermodynamics-antioxidant activity relationships of selected natural phenolic acids and derivatives: An experimental and theoretical evaluation. *PLoS One* **2015**, *10* (3), No. e0121276, DOI: 10.1371/journal.pone.0121276.
(50) Prior, R. L.; et al. Standardized methods for the determination of antioxidant capacity and phenolics in foods and dietary supplements. *J. Agric. Food Chem.* **2005**, *53* (10), 4290−4302, DOI: 10.1021/jf0502698.
(51) Drzeżdżon, J.; et al. Relationship between antioxidant activity and ligand basicity in the dipicolinate series of oxovanadium (IV) and dioxovanadium (V) complexes. *Int. J. Mol. Sci.* **2021**, *22* (18), 9886 DOI: 10.3390/ijms22189886.
(52) Purcell, K. F.; Yeh, S. M.; Eck, J. Magnetic isomers of iron (II). Bis (C-cyanotrihydroborate) bis (phenanthroline) iron-a spin triplet. *Inorg. Chem.* **1977**, *16* (7), 1708−1715, DOI: 10.1021/ic50173a028.
(53) Manna, D.; Ghanty, T. Complexation behavior of trivalent actinides and lanthanides with 1, 10-phenanthroline-2, 9-dicarboxylic acid based ligands: insight from density functional theory. *Phys. Chem. Chem. Phys.* **2012**, *14* (31), 11060−11069, DOI: 10.1039/c2cp40083a.
(54) Lein, M.; et al. Energy decomposition analysis of the chemical bond in main group and transition metal compounds. *Faraday Discuss.* **2003**, *124*, 365−378, DOI: 10.1039/B300066B.
(55) Frenking, G.; Solà, M.; Vyboishchikov, S. F. Chemical bonding in transition metal carbene complexes. *J. Organomet. Chem.* **2005**, *690* (24−25), 6178−6204, DOI: 10.1016/j.jorganchem.2005.08.054.

https://doi.org/10.1021/acsomega.3c07885
ACS Omega 2024, 9, 9076−9089